Neural Computing and Applications (2021) 33:5753–5769
https://doi.org/10.1007/s00521-020-05355-y

ORIGINAL ARTICLE

Integrated neuro-evolution-based computing solver for dynamics of nonlinear corneal shape model numerically

Iftikhar Ahmad[1] · Muhammad Asif Zahoor Raja[2,3] · Higinio Ramos[4] · Muhammad Bilal[5] · Muhammad Shoaib[6]

Received: 25 March 2020 / Accepted: 8 September 2020 / Published online: 17 September 2020

Abstract

In this study, bio-inspired computational techniques have been exploited to get the numerical solution of a nonlinear two-point boundary value problem arising in the modelling of the corneal shape. The computational process of modelling and optimization makes enormously straightforward to obtain accurate approximate solutions of the corneal shape models through artificial neural networks, pattern search (PS), genetic algorithms (GAs), simulated annealing (SA), active-set technique (AST), interior-point technique, sequential quadratic programming and their hybrid forms based on GA–AST, PS–AST and SA–AST. Numerical results show that the designed solvers provide a reasonable precision and efficiency with minimal computational cost. The efficacy of the proposed computing strategies is also investigated through a descriptive statistical analysis by means of histogram illustrations, probability plots and one-way analysis of variance.

Keywords Stochastic numerical computing · Neural networks · Genetic algorithms · Corneal shape models · Optimization techniques

✉ Higinio Ramos
higra@usal.es

Iftikhar Ahmad
dr.iftikhar@uog.edu.pk

Muhammad Asif Zahoor Raja
rajamaz@yuntech.edu.tw

Muhammad Bilal
PSE15004@stdmail.ump.edu.my

Muhammad Shoaib
dr.shoaib@cuiatk.edu.pk

[1] Department of Mathematics, University of Gujrat, Gujrat, Pakistan

[2] Future Technology Research Center, National Yunlin University of Science and Technology, 123 University Road, Section 3, Douliou 64002, Yunlin, Taiwan, ROC

[3] Department of Electrical and Computer Engineering, COMSATS University Islamabad, Attock Campus, Attock 43600, Pakistan

[4] Department of Applied Mathematics, University of Salamanca, Salamanca, Spain

[5] Faculty of Science and Technology, University of Malaysia Pahang, Pekan, Malaysia

[6] Department of Mathematics, COMSATS University Islamabad, Attock Campus, Attock 43600, Pakistan

1 Introduction

Vision is an essential sense in humans and many animals. It is a fundamental issue for better understanding of biology, as well as the physics of sight for dealing with different diseases during treatment. The eye in the human body has a significant role of sight; two-thirds of its refractive power are due to its Cornea, which is commonly known as the front part of the eye. Researchers have contributed significantly to have a detailed knowledge of corneal anatomy and its optics (see [1]). The Cornea is considered to be highly sensitive, and many sight disorders may be due to a change in the corneal shape and its geometry. Possibly, an incorrect corneal geometry is partly responsible for some common diseases like astigmatism, hyperopia and myopia. The accuracy of refractive surgery and adjustment of contact lens is usually subject to a deep understanding of the corneal topography and models [2–5]. Therefore, for a better ophthalmological use, a detailed knowledge and information of the corneal shape are of paramount importance.

Researchers have conducted several investigations on mathematical models for corneal shape [6]. Some studies

address the variable eccentricity ratio of the conics based on a complex shell theory model that describes its mathematical interpretation [7]. The corneal biomechanical behaviour is investigated through a finite element modelling [8]. Zernike polynomial approximations are used for corneal geometry modelling [9]. Models with rational functions for video keratoscopy compression have been used [10], and a Fourier series method (FSM) to identify the crystalline lens shape has been considered [11]. In general, the efficiency of the physical models of the eye is greatly improved through the use of theoretical and mathematical considerations [12, 13]. These models help to develop the equipments used in medicine without the involvement of patients. Recently, a few scientists have investigated collagen fibrils in soft tissues and have developed a class of models that illustrates the biomechanics of the Cornea [14].

In this study, a mathematical model of the corneal shape based on a nonlinear differential equation is studied, which provides an effective solution to address different diseases of the Cornea. The nonlinear corneal shape model (NCSM) is represented by means of a two-point boundary value problem (BVP) of second-order ordinary differential equation (ODE) as:

$$\frac{\mathrm{d}}{\mathrm{d}x}\left(\frac{\mathrm{d}u}{\mathrm{d}x}\Big/\sqrt{1+\left(\frac{\mathrm{d}u}{\mathrm{d}x}\right)^2}\right)-au(x)+b\Big/\sqrt{1+\left(\frac{\mathrm{d}u}{\mathrm{d}x}\right)^2}=0,$$
$$x\in[0,1], a>0, b>0,\quad u'(0)=0, u(1)=0, \tag{1}$$

where the curve u(x) = 0 represents a meridian of a surface of revolution related to the corneal geometry, while a and b are positive real constants. The N-dimensional counterpart of model (1) is given as follows:

$$\begin{cases} u=0 & \text{on } \Omega \\ \operatorname{div}\left(\dfrac{\nabla u}{\sqrt{1+|\nabla u|^2}}\right)=au-\dfrac{b}{\sqrt{1+|\nabla u|^2}}, & \text{in } \Omega \end{cases} \tag{2}$$

The models in Eqs. (1–2) have been proposed as suitable models of the geometry of the human Cornea in [1–4]. However, in these studies, a simplified version of the above model has been investigated with the replacement of the mean curvature term $\operatorname{div}\left(\nabla u\Big/\sqrt{1+|\nabla u|^2}\right)$ by its linearization, $\operatorname{div}(\nabla u)$, in a neighbourhood of 0.

As a particular case, when $b\in\left]0,\frac{3\sqrt{3a}}{2\tanh\sqrt{a}}\right[$, the NCSM equation in (1) is modified as:

$$\begin{cases} u''-au+\dfrac{b}{\sqrt{1+u'^2}}=0 \\ u'(0)=0,\quad u(1)=0 \end{cases} x\in[0,1], \tag{3}$$

The existence of a unique solution for the problem in (3) has been proven in [4].

To obtain the best refractive properties of the Cornea by using such type of models (3), the Cornea geometry must be shell-like with diameter 11 mm, inner thickness 0.5 mm and peripheral part 0.7 mm [15]. Moreover, the Cornea constructs a mechanical shield inside the eye for its durability [16, 17]. A schematic diagram of the human eye anatomy showing the corneal shape is displayed in Fig. 1.

The Cornea has five different layers from the outermost to the innermost; these layers are epithelium, Bowman's layer, stroma, fourth Descement's membrane and the last one known as endothelium. Each layer differs from another due to its own biological properties. For example, the 90% of the corneal thickness is due to stroma layer, which has great importance in optics and for identifying purposes. The reported studies to solve the corneal shape model are based on renewed deterministic numerical procedures. Nevertheless, stochastic computational techniques based on artificial neural networks (ANNs) optimized by genetic algorithms (GA), i.e. based on global search methods, have been used to solve broad nonlinear systems [18, 19] but they have not been applied yet for solving the nonlinear corneal shape models arising in bioinformatics. In addition, these approaches have many advantages over traditional numerical schemes, since they provide a continuous solution over the domain of training inputs, their computational requirements do not dependent upon sample size, and through interpolation one can find the solution at any point outside the trained interval.

ANNs have been applied to many problems modelled by linear and nonlinear systems [20–25]. Recently, stochastic solvers were used broadly in nanotechnology problems [26], optimization of nonlinear prey–predator systems [27], nonlinear pantograph systems [28],

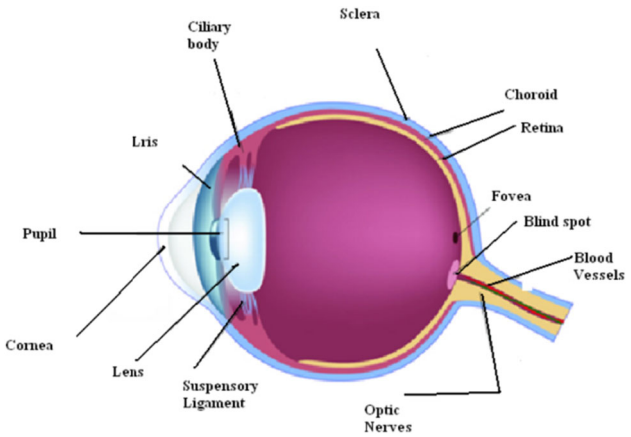

Fig. 1 Human eye anatomy

distribution of heat in porous fin models [29], solution for micropolar fluid flow problem [30], models of electrical conducting solids [31], mathematical problem arising in electromagnetic theory [32], Bratu systems arising in fuel ignition model [33], nonlinear Troesch's problems [34, 35], astrophysics [36], nonlinear electrical circuit [37], atomic physics [38], thermodynamics [39], nonlinear optics [40], heartbeat models [41], HIV infection studies [42], mathematical model for wire coating analyses [43], nonlinear Painlevé II systems [44], nonlinear elliptic BVPs [45], fractional order Bagley–Torvik systems [46], nonlinear Falkner–Skan systems [47], nonlinear Flierl–Petviashivili system [48] and fractional order system of Riccati equation [49]. These are motivating factors to study the dynamics of the nonlinear corneal shape problem using ANNs and their optimization with standalone solver including interior-point technique (IPT), active-set technique (AST), sequential quadratic programming (SQP), genetic algorithm (GA), simulating annealing (SA) and pattern search (PS), as well as their hybrid combinations through the SA–AST, PS–AST and GA–AST. The efficiency of these techniques is evaluated through detailed statistical analyses that include one-way analysis of variance (ANOVA). The presented study is a novel investigation in intelligent computing paradigm to determine the approximate solution of the nonlinear corneal shape models. The salient features of this study are summarized as follows:

- Novel application of bio-inspired computational techniques has been presented for the numerical solution of BVPs arising in the modelling of the corneal shape.
- The computational process of modelling and optimization is exploited to obtain accurate solutions for governing relations of NCSM through ANNs, GAs, PS, SA, IPT, AST, SQP and their hybrids PS–AST, GA–AST and SA–AST.
- The convergence study through multiple autonomous trials is conducted to authenticate the performance of the stochastic methodologies to obtain an effective, reliable and stable solution of the corneal geometry.
- Statistical assessments through ANOVA testing further validate a better precision and convergence of computing solvers.

The rest of the paper is organized as follows. Design methodology for NCSM by means of ANN-based differential equation models and learning methodologies is presented in Sect. 2. Results of numerical experimentations for NCSM along with necessary interpretations are presented in Sect. 3. Some concluding remarks along with future recommendations are given in Sect. 4.

2 Design methodology for NCHM

The proposed designed scheme for solving the NCHM is presented here in two parts; firstly, the mathematical modelling of NCHM is presented with the help of neural networks, while in the second part, optimization schemes are introduced, which are used for finding the decision variables of the networks. The workflow of the proposed design procedure is shown in Fig. 2.

2.1 Mathematical modelling for NCHM

In this section, mathematical modelling used for the solution of the two-point nonlinear BVP arising in the model of the corneal shape is presented. The approximate ANN solution is developed by using the continuous mapping of the solution $u(x)$ and its derivatives as follows:

$$\begin{cases} \hat{u}(x) = \sum_{i=1}^{m} \delta_i f(\beta_i + \omega_i x) \\ \dfrac{\mathrm{d}\hat{u}(x)}{\mathrm{d}x} = \sum_{i=1}^{m} \delta_i \dfrac{\mathrm{d}}{\mathrm{d}x} f(\beta_i + \omega_i x) \\ \vdots \\ \dfrac{\mathrm{d}^n \hat{u}(x)}{\mathrm{d}x^n} = \sum_{i=1}^{m} \delta_i \dfrac{\mathrm{d}^n}{\mathrm{d}x^n} f(\beta_i + \omega_i x) \end{cases}, \tag{4}$$

where $\hat{u}(x)$ denotes the estimated solutions and $W = [\delta_i, \beta_i, \omega_i],\ i = 1, 2, 3 \ldots, m.$ are weights of the ANN model with m neurons and f is the log-sigmoid activation function. The weights W of the ANN in (4) are the decision variables of the optimization mechanism used for training. Additionally, these weights W are optimization variables represented with arbitrary real numbers in a bounded domain. The effectiveness of log-sigmoid as an activation function in hidden layers of ANNs (4) is well proven over other counterparts due to its rapid convergence rates, better windowing characteristics and stability [50, 51].

The networks in (4) up to second-order derivatives can be written as follows:

$$\begin{cases} \hat{u}(x) = \sum_{i=1}^{m} \dfrac{\delta_i}{1 + \mathrm{e}^{(-\omega_i x - \beta_i)}} \\ \hat{u}'(x) = \sum_{i=1}^{m} \dfrac{\delta_i \omega_i}{2(1 + \cosh(\omega_i x + \beta_i))} \\ \hat{u}''(x) = \sum_{i=1}^{m} \delta_i \omega_i^2 \left(-2\mathrm{csch}(\omega_i x + \beta_i)^3 \sinh\left(\dfrac{\omega_i x + \beta_i}{2} \right)^4 \right). \end{cases} \tag{5}$$

The networks in the set of Eqs. (5) are arbitrarily combined to represent the differential equation along with its boundary conditions, where the decision variables of the system depend upon the weights of ANNs. The fitness

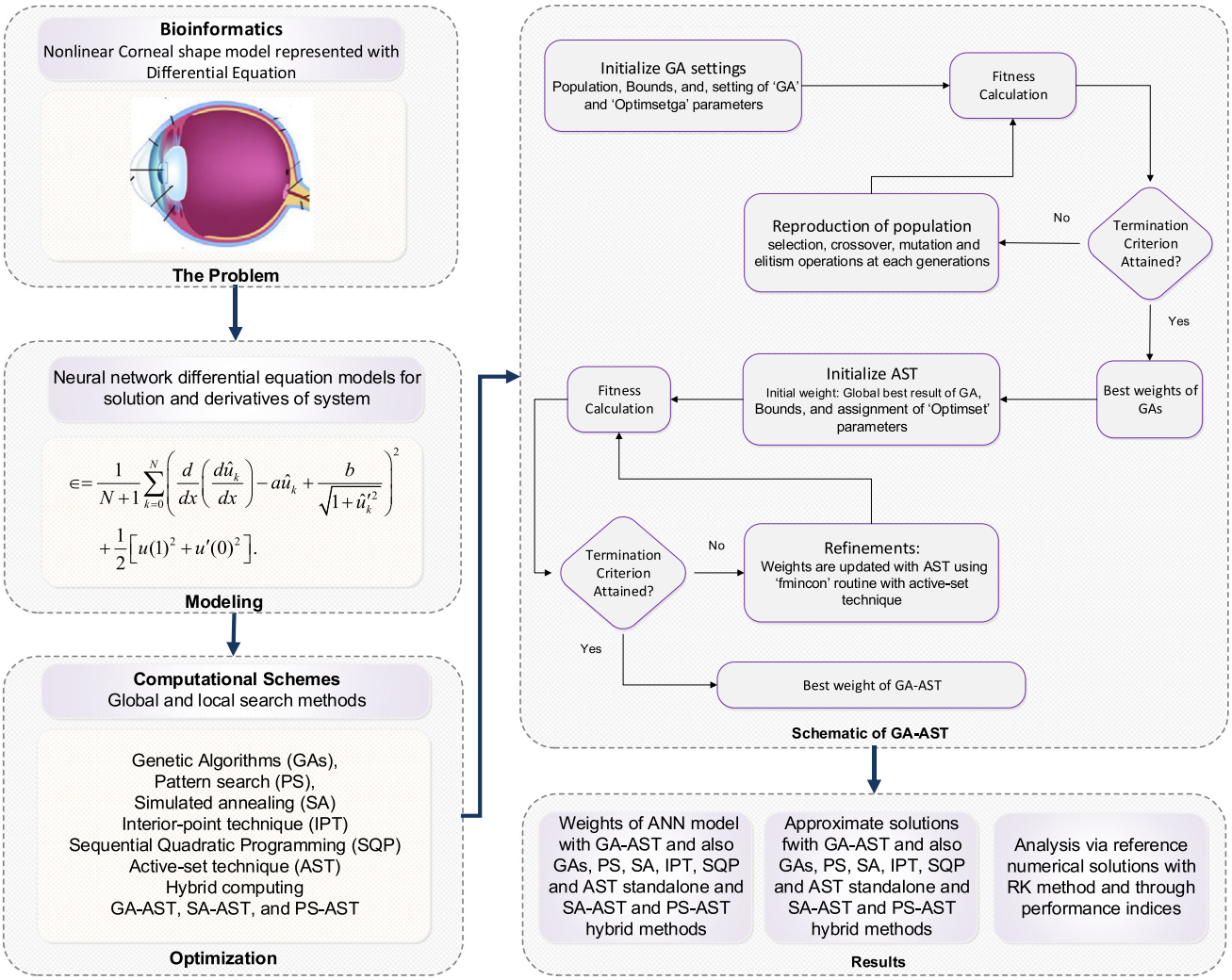

Fig. 2 Generic workflow of hybrid computing methods for nonlinear corneal shape model

function is computed by defining two mean-square errors of the two-point BVP for the corneal shape model as

$$\in = \in_1 + \in_2 \ . \tag{6}$$

$$\in_1 = \frac{1}{N+1}\sum_{k=0}^{N}\left(\hat{u}_k'' - a\hat{u}_k + \frac{b}{\sqrt{1+\hat{u}_k'^2}}\right)^2, \tag{7}$$

$$\in_2 = \frac{1}{2}\left[\hat{u}(1)^2 + \hat{u}'(0)^2\right] \tag{8}$$

$$\in = \frac{1}{N+1}\sum_{k=0}^{N}\left(\hat{u}_k'' - a\hat{u}_k + \frac{b}{\sqrt{1+\hat{u}_k'^2}}\right)^2 + \frac{1}{2}\left[\hat{u}(1)^2 + \hat{u}'(0)^2\right]. \tag{9}$$

Our main goal is to minimize the value $\in$ by searching suitable weights of the network in (5) for which the value $\in$ approaches zero, i.e. $\in \to 0$. Thus, accordingly, the obtained solution $\hat{u}$ will approximate the reference exact solution u of the BVP that models the corneal shape. The fitness function represented in Eq. (9) is presented in the layered structure of neural networks as shown in Fig. 3.

2.2 Learning techniques

In this section, a brief overview of optimization schemes AST, IPA, SQP, PS, SA and GA for ANN models is presented.

AST, SQP and IPTs belong to a class of local search methodologies that were exploited effectively for constrained and unconstrained optimization tasks [52]. In the procedure of both AST and SQP algorithms, the given optimization task is segmented/transformed into relatively easier sub-problems and procedures mainly based on Karush–Kuhn–Tucker conditions, which are adopted for iterative refinements. The IPT iteratively updates the weights by exploiting the feasible interior region of the

optimization problem. The AST, SQP and IPT have been widely applied to many stiff and non-stiff optimization problems of practical interest (see [53, 54] and references cited therein).

The SA technique is a simple computational technique based on two characteristics of material, i.e. controlled cooling process and meticulous heating [55, 56]. The main objective of SA method is to adjust the approximate solutions successfully and effectively within a controlled interval of time. Complex optimization problems can be solved through the SA technique, and thus, it is widely applied by researchers in optimization of vehicle routing problem [57], capacitated vehicle routing problem with 2D loading constraints [58] and optimization of machine scheduling problem [59].

The PS technique is known for working without prior knowledge of the gradient of the function. This technique was proposed firstly by Hooke and Jeeves [60], while Yu was the first one to provide the convergence of the PS method with the help of the theory of positive bases [61]. The PS technique process through a set of patterns called mesh points in the close vicinity of the optimal location [62]. The PS method has been also used as a convenient procedure for the solution of optimization problems with bounded as well as linear constraints (see [60–63] and references cited therein).

A GA was firstly presented to simulate a simple picture of the natural selection by Holland [64], and its performance was subject to appropriate selection of data of the initial population, suitable choices for chromosomes to the next generation, survival of valuable genes to provide the seed for the next generation (called mutation). The GAs work on the evolutionary principle and are widely used by many researchers in stiff optimization tasks by exploiting its characteristic of robustness, avoidance of local minimum with moderate, divergence-free adaptation and consistent as compared to other counterparts [65–68].

In the present study, the optimization task is performed in the MATLAB environment using algorithms available in the graphical user interface optimization toolbox based on IPT, AST, SQP, PS, SA, GA, PS–SQP, SA–SQP and GA–SQP. The procedural process blocks of the proposed scheme are presented in Fig. 2, while the settings of the parameters are given in Table 1. Additionally, the pseudocode of the optimization procedure is given in Algorithm 1.

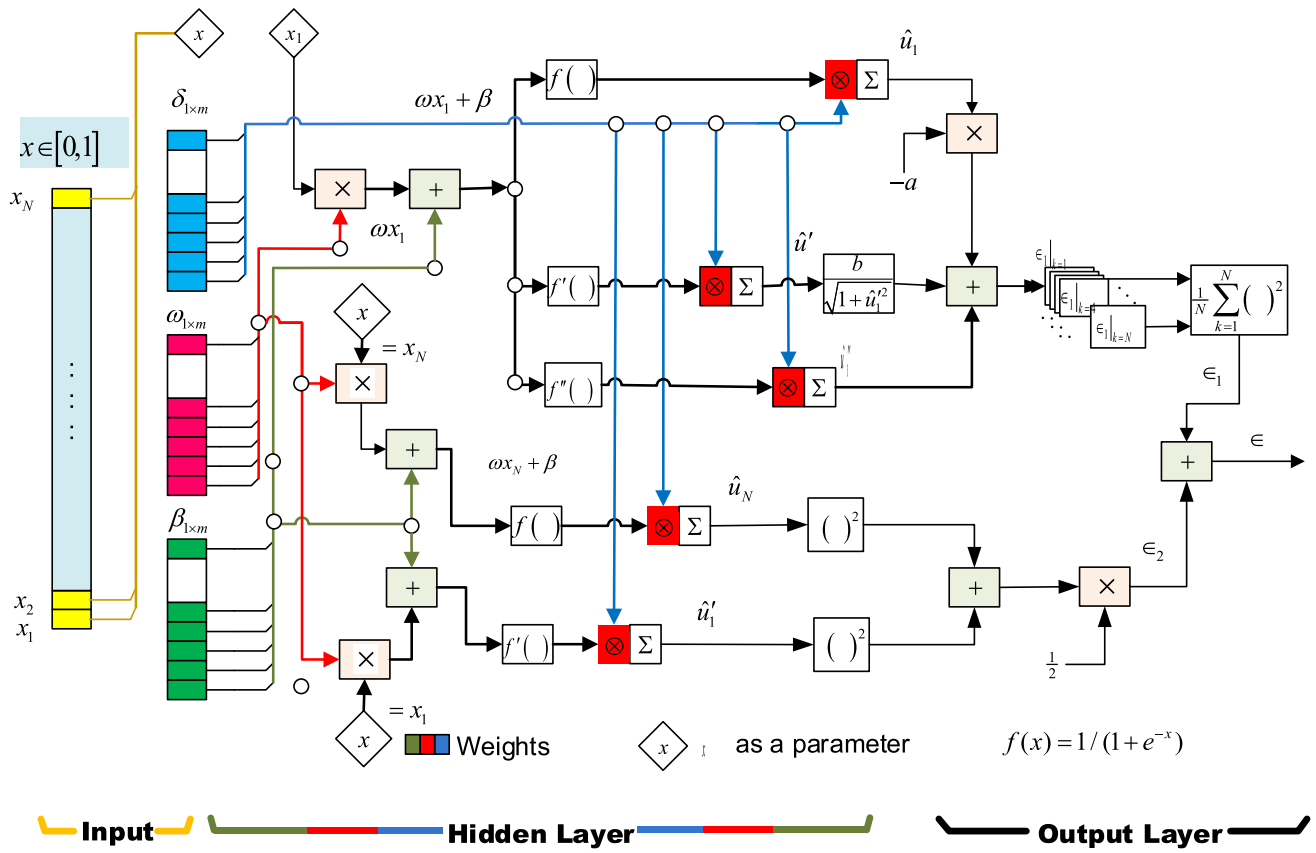

Fig. 3 Layered structure of neural network models for nonlinear corneal shape model

Algorithm 1: Pseudocode optimization mechanism

Step-1: *Initialization*: Create the start-up population data with real entries based on the number of neurons in ANN models randomly. Each row vector of the population contains a number of elements equal to the number of weights in the ANN model. In Table 1, the settings used for the parameters of GA solver are tabulated.
Step-2: *Fitness evaluations*: The fitness values using equations (6-9) is calculated for each individual, i.e., row vector of the population.
Step-3: *Termination conditions*: Stop the optimization of GA based solver when it meets any of the conditions stated below:

- Fitness limit is attained, *i.e.*, $\in \leq 10^{-10}$
- Iterations/generations limit is attained.

If the above criteria are satisfied, then go to the step 6 for further refinements.
Step-4: *Ranking*: Ranking of the individuals via the minimum value of mean squared error fitness.
Step-5: *Reproduction*: The reproduction is the process of getting new population data. Reproduction is performed by using the selection, crossover and mutation, operations according to the setting tabulated in Table 1.
Then proceed from step-2: fitness evaluations with updated population.
Step-6: *Refinements*: To get speedy improvement in GA results/optimized values, local search processes with AST, IPT and SQP algorithms is exploited. The individuals with a minimum value of fitness by GAs are fed to AST, SQP and IPT as initial optimization variables or start points.
Step-7: *Storage of data*: Store the global best weight vectors for each standalone and hybrid algorithm.
Step-8: *Statistic*: Perform a sufficient number of runs for each solver by repeating steps 1 to 7. The stored dataset is used for detailed statistical analyses.

3 Results and discussion

The ANN-based proposed method is applied for computing the solution of the corneal shape model (3) with unit value of coefficient a and b as

$$\begin{cases} u'' - au + \dfrac{b}{\sqrt{1+u'^2}} = 0, & x \in [0,1], \\ u'(0) = 0, \;\; u(1) = 0, \end{cases}$$

The proposed standalone computing algorithms, i.e. SQP, AST, IPT, PS, GA and SA, as well as hybrid procedures, i.e. GA–AST, PS–AST and SA–ASTs, are applied to find the weights to solve the corneal shape model with the parameter settings given in Table 1 and procedure presented in Algorithm 1. The graphical representation of trained weights in terms of three-dimensional and two-dimensional plots is shown in Figs. 4 and 5, respectively, while numerical results are shown in Table 2.

The approximate solutions $\hat{u}_{\mathrm{GA-AST}}$, $\hat{u}_{\mathrm{PS-AST}}$ and $\hat{u}_{\mathrm{SA-AST}}$ are obtained for a number of 10 neurons in ANN and with the help of weights trained by hybrid optimization

Table 1 Parameter settings of the local and global search algorithms

AST/SQP/IPTs		PS		GA		SA	
Index	Set	Index	Set	Index	Set	Index	Set
Initial weight vectors	Randomly (1,1)	Solver	PS	Ini penalty	10	Max Itera	100,000
Number of variables	30	Start point	Random (1,30)	Penalty factor	100	Max Fun Eval	10^7
Iteration limit	1000	Poll method	GPS positive 2 N	Crossover rate	0.8	Time limit	Inf
Function count limit	100,000	Complete Poll	Off	Population size	200	FunTol	C
Derivative	By solvers	Polling order	Connective	Mutation rate	0.1	Stall Itera	10^8
Finite difference	Central	Initial Size	1	Elite count	2	Anneali Fun	Fast
Hessian	BFGS	Max iteration	10^6	Time limit	Inf	Initial Temp	100
Algorithm	AST/SQP/IPA	Max Fun Eval	10^7	Scaling Fun	Rank	Data type	Double
Others	Sefaults	Others	Defaults	Others	Defaults	Others	Defaults

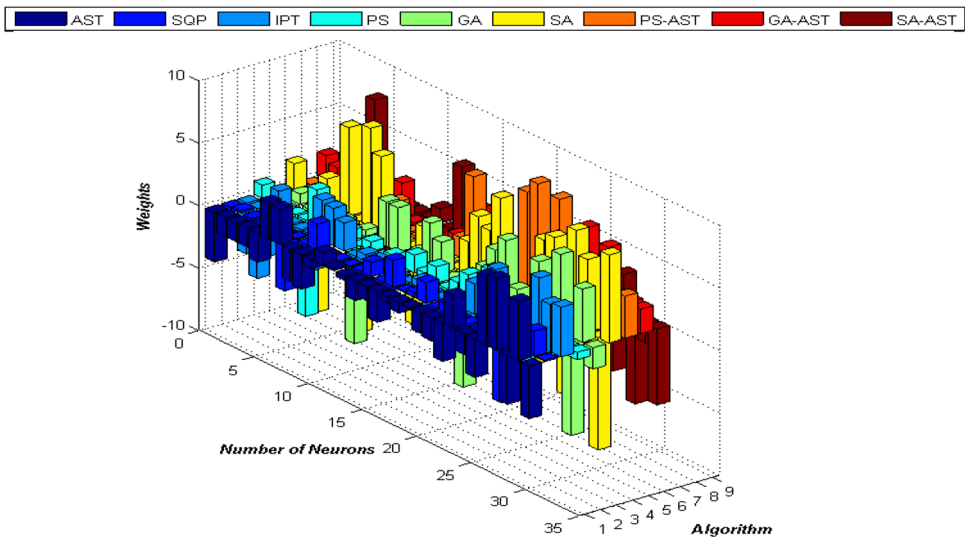

Fig. 4 Three-dimensional representation of weights of ANNs optimized with the proposed schemes

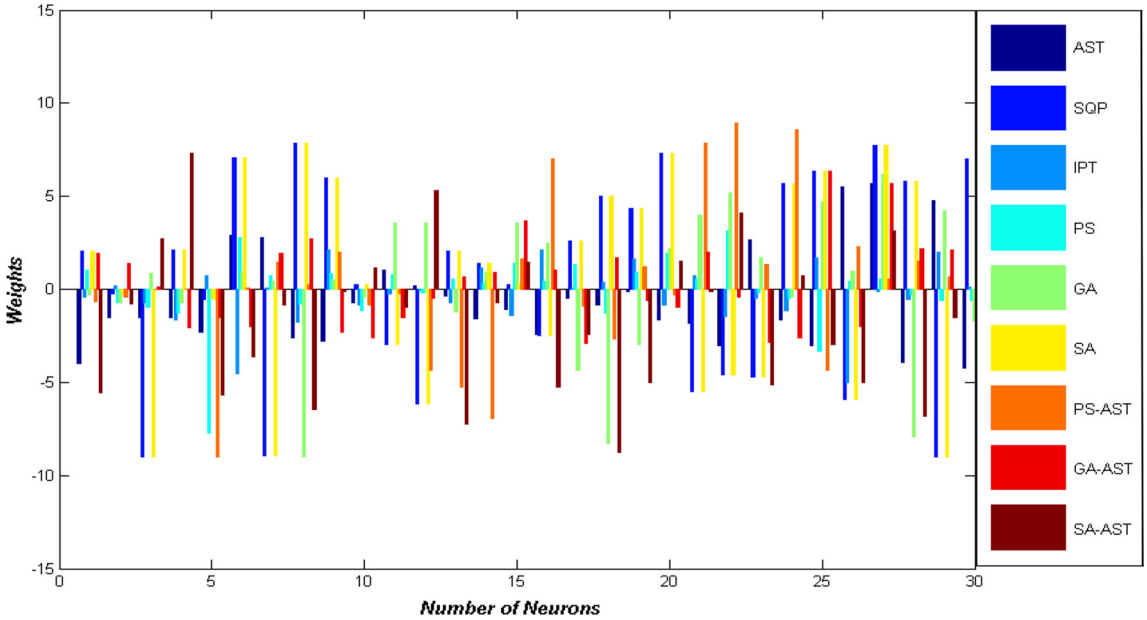

Fig. 5 Two-dimensional representation of weights of ANN optimized with proposed schemes

procedures based on GA–AST, PS–AST and SA–AST as listed in Table 2. These solutions are given by

$$\hat{u}_{\mathrm{GA-AST}}(x) = \frac{1.947736}{1+e^{(1.49876+2.020087x)}} + \frac{1.396893}{1+e^{(.47495+.39565x)}} + \cdots + \frac{-2.59037}{1+e^{(.94018-1.969659x)}} \tag{10}$$

$$\hat{u}_{\mathrm{PS-AST}}(x) = \frac{-0.625902}{1+e^{(.25572-7.853314x)}} + \frac{-0.40317}{1+e^{(4.35784+8.957554x)}} + \cdots + \frac{-.86932}{1+e^{(.28391-3.368182x)}} \tag{11}$$

$$\hat{u}_{\mathrm{SA-AST}}(x) = \frac{-5.5354}{1+e^{(0.95399+0.12536x)}} + \frac{-.78324}{1+e^{(-5.3268+4.116746x)}} + \cdots + \frac{1.153815}{1+e^{(-1.47945+6.04943x)}} \tag{12}$$

The solutions provided by Eqs. (10–12) can be calculated with reasonable accuracy for continuous values in [0, 1] and are presented numerically in Table 3, while their graphical representations are shown in Fig. 6.

The values of absolute errors (AEs), i.e. $|u(x) - \hat{u}(x)|$, are also determined for the proposed algorithms from the reference solution provided with an implicit RK method with the help of Mathematica using the built-in software

Table 2 A set of weight vectors of ANN models of differential equation for each optimization solver

Index	i	δ_i	β_i	ω_i	Index	δ_i	β_i	ω_i	Index	δ_i	β_i	ω_i
AST	1	− 3.96646	1.022565	− 1.82457	GA	− 0.30121	3.574531	3.972703	GA–AST	1.947736	− 1.49876	2.020087
	2	− 1.49755	0.180213	− 3.01115		− 0.69865	3.541485	5.165102		1.396893	− 0.47495	− 0.39565
	3	− 1.48461	− 0.36457	2.659874		0.832771	− 1.179	1.66844		0.119611	0.691062	− 2.80767
	4	− 1.49961	− 1.55929	− 1.61475		− 0.69461	0.911268	− 0.39791		− 2.07582	0.881066	− 2.57213
	5	− 2.29646	− 1.11091	− 3.02818		− 0.46188	3.587577	4.736476		− 1.49008	3.663348	6.359995
	6	2.86772	− 2.44441	5.478431		0.883617	2.490846	0.955247		− 1.96891	1.039351	− 1.96976
	7	2.79236	− 0.48905	5.700075		0.435944	− 4.3249	6.177993		1.9492	− 2.87288	5.646111
	8	− 2.57367	− 0.85613	− 3.90172		− 8.99974	− 8.24864	− 7.87941		2.701937	1.696135	2.154909
	9	− 2.75920	− 0.09798	4.744912		0.504732	− 2.95379	4.233898		− 2.27169	− 0.62682	2.102439
	10	− 0.70139	− 1.64234	− 4.21104		− 0.4009	2.186391	− 1.70591		− 2.59037	− 0.94018	1.969659
IPT	1	− 0.39894	− 0.22968	0.723449	PS	1.053305	0.764251	0.541139	PS–AST	− 0.63592	− 0.25572	7.853314
	2	0.18146	− 0.08628	− 1.42129		− 0.74888	− 0.15292	3.161271		− 0.40327	− 4.35784	8.957554
	3	− 0.70362	− 0.71003	− 0.46628		− 0.93633	0.557055	− 0.20314		0.00865	− 5.23843	1.308866
	4	− 1.60044	1.128507	− 1.16681		− 1.26909	0.315986	− 0.49997		− 0.00885	− 6.94007	8.559043
	5	0.71941	− 1.37703	1.71675		− 7.74494	1.406535	− 3.3118		− 8.99325	1.657743	− 4.35326
	6	− 4.53611	2.128688	− 5.01581		2.789081	0.401125	0.412035		0.05001	6.978688	2.271106
	7	0.075523	0.078634	− 0.12908		0.727572	1.31882	0.541235		1.473226	− 0.90195	0.514682
	8	− 1.76633	0.387911	− 0.51412		− 0.77306	− 1.27206	− 0.30714		0.230114	− 2.6849	1.521032
	9	2.088403	1.652404	1.98567		0.836634	0.905677	− 0.59927		2.005237	1.236894	0.65099
	10	− 0.81541	− 0.85918	0.096408		− 1.12833	1.945143	− 0.58959		− 0.86932	− 0.28391	3.368132
SQP	1	− 4.06998	− 1.33894	− 1.72176	SA	2.035377	− 2.98494	− 5.49515	SA–AST	− 5.5354	− 0.95399	− 0.12536
	2	− 5.5992	0.546935	2.432942		− 0.24945	− 6.1507	− 4.58537		− 0.78324	5.326876	4.116746
	3	− 3.41794	0.538541	− 1.87925		− 8.99991	2.033149	− 4.70641		2.711177	− 7.25435	− 5.13404
	4	2.204084	− 1.26816	4.428297		2.088723	1.399349	5.697294		7.295543	− 0.69485	0.73613
	5	− 2.64745	− 0.11102	1.251217		− 0.56258	0.248299	6.322197		− 5.64905	1.434658	− 2.97686
	6	− 2.7623	− 0.33959	− 0.89915		7.04195	− 2.49635	− 5.89234		− 3.61618	− 5.27741	− 5.02515
	7	− 2.87106	0.556301	− 0.82027		− 8.93566	2.607322	7.724387		− 0.81839	− 2.38578	3.114661
	8	3.175688	− 2.16235	5.446253		7.838256	5.014942	5.821357		− 6.46436	− 8.75103	− 6.81594
	9	2.96976	− 0.9602	3.765901		5.992892	4.351193	− 8.97509		− 0.10695	− 5.01275	− 1.49606
	10	2.230227	− 1.02349	3.956452		0.21833	7.302268	7.03006		1.153815	1.479459	− 6.04943

Table 3 Comparative analysis from the reference numerical solution

Inputs	Reference results	Proposed solutions								
x	Numerical	$\hat{u}_{\text{AST}}$	$\hat{u}_{\text{IPT}}$	$\hat{u}_{\text{SQP}}$	$\hat{u}_{\text{PS}}$	$\hat{u}_{\text{GA}}$	$\hat{u}_{\text{SA}}$	$\hat{u}_{\text{PS-AST}}$	$\hat{u}_{\text{GA-AST}}$	$\hat{u}_{\text{SA-AST}}$
0.0	0.484338	0.47865	0.478656	0.47865	0.478802	0.479218	0.480466	0.478657	0.478666	0.478631
0.1	0.478773	0.473978	0.473984	0.473978	0.474121	0.47452	0.477676	0.473985	0.473993	0.473962
0.2	0.463957	0.459963	0.459967	0.459963	0.460072	0.460469	0.467959	0.459969	0.459975	0.459952
0.3	0.439879	0.436595	0.436598	0.436596	0.436676	0.437133	0.449426	0.436601	0.436606	0.436586
0.4	0.406504	0.403843	0.403845	0.403843	0.40392	0.404398	0.421233	0.403846	0.40385	0.403832
0.5	0.363748	0.361626	0.361628	0.361626	0.361712	0.362141	0.382983	0.361627	0.36163	0.361616
0.6	0.311452	0.3098	0.309802	0.309799	0.309879	0.310292	0.334443	0.309802	0.309804	0.309794
0.7	0.249355	0.248133	0.248134	0.248132	0.248186	0.248696	0.275409	0.248136	0.248137	0.248131
0.8	0.17709	0.176283	0.176285	0.176283	0.176325	0.17697	0.205622	0.176285	0.176286	0.176282
0.9	0.094159	0.093779	0.09378	0.09378	0.093836	0.094521	0.124717	0.09378	0.09378	0.093777
1.0	0.00E+00	5.40E−08	5.46E−07	1.32E−08	4.33E−05	6.95E−04	0.03215	2.27E−09	1.15E−07	8.87E−08

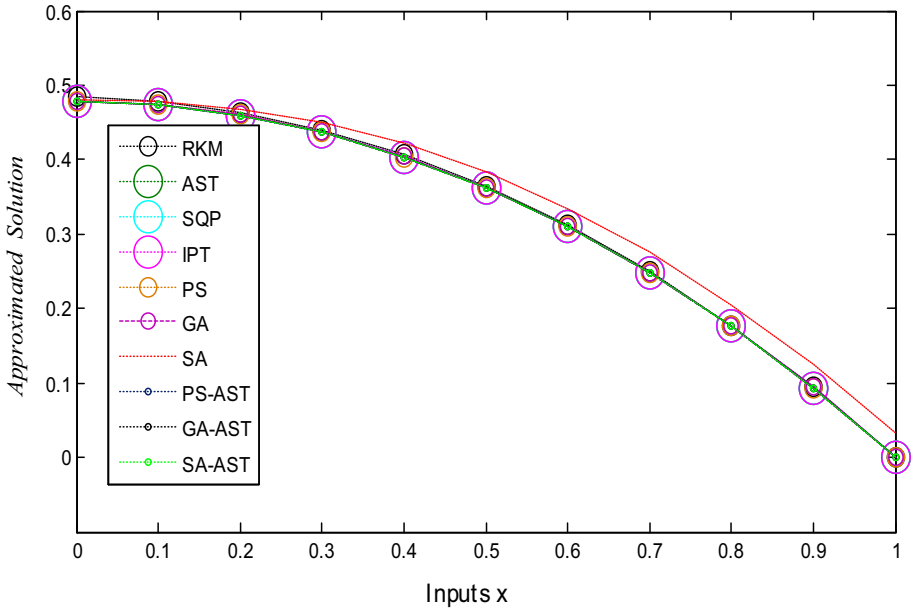

Fig. 6 Graphical representation of the approximate solutions along with reference solution

package "NDSolve" with default values of adaptive step size, accuracy goal and tolerances. The results are given in Table 4, while their graphical representation is shown in Fig. 7 for inputs in the interval [0,1] with step size 0.1. The detailed statistical observations for 100 independent runs of each solver are tabulated in Table 5, while the fitness values are shown in Fig. 8 for the considered problem for each stochastic numerical solver.

From the results of detailed simulations, it is observed that the AEs are in the range 10^{-03}–10^{-08}, for AST; 10^{-03}–10^{-07} for SQP; 10^{-03}–10^{-06} for IPT; 10^{-02}–10^{-03} for PS; 10^{-02}–10^{-03} for GA; 10^{-02}–10^{-03} for SA; 10^{-03}–10^{-09} for PS–AST; 10^{-03}–10^{-08} for GA–AST and 10^{-03}–10^{-09} for SA–AST. The mean value of AEs (MAE) is calculated by the formula

$$\text{MAE} = \frac{1}{11}\sum_{i=0}^{10} |u(x_i) - \hat{u}(x_i)|, \tag{13}$$

and the values of MAE for each optimization solver are shown in Fig. 9. It is seen that the MAEs for standalone approaches AST, SQP, IPT, PS, GA and SA are in the range 10^{-01}–10^{-04}, while for the hybrid methodologies PS–AST, GA–AST and SA–AST are in the range 10^{-05}–10^{-07}.

Table 4 Comparative analysis on AEs from the reference numerical solution

Inputs	Values of absolute error for algorithms								
x	AST	IPT	SQP	PS	GA	SA	PS–AST	GA–AST	SA–AST
0.0	5.69×10^{-3}	5.69×10^{-3}	5.69×10^{-3}	2.21×10^{-3}	3.87×10^{-3}	4.76×10^{-3}	6.81×10^{-3}	5.69×10^{-3}	5.69×10^{-3}
0.1	4.80×10^{-3}	4.79×10^{-3}	4.80×10^{-3}	1.65×10^{-3}	2.94×10^{-3}	6.01×10^{-3}	4.79×10^{-3}	4.80×10^{-3}	4.79×10^{-3}
0.2	3.99×10^{-3}	3.99×10^{-3}	3.40×10^{-3}	1.30×10^{-3}	2.13×10^{-3}	5.04×10^{-3}	3.40×10^{-3}	4.00×10^{-3}	3.99×10^{-3}
0.3	3.28×10^{-3}	3.28×10^{-3}	3.29×10^{-3}	8.92×10^{-4}	1.57×10^{-3}	3.28×10^{-3}	3.28×10^{-3}	3.29×10^{-3}	3.28×10^{-3}
0.4	2.66×10^{-3}	2.66×10^{-3}	2.67×10^{-3}	4.26×10^{-4}	1.22×10^{-3}	1.65×10^{-3}	2.66×10^{-3}	2.67×10^{-3}	2.66×10^{-3}
0.5	2.12×10^{-3}	2.12×10^{-3}	2.13×10^{-3}	3.92×10^{-5}	9.41×10^{-4}	5.95×10^{-4}	2.12×10^{-3}	2.13×10^{-3}	2.12×10^{-3}
0.6	1.65×10^{-3}	1.65×10^{-3}	1.66×10^{-3}	2.56×10^{-4}	5.87×10^{-4}	2.27×10^{-4}	1.65×10^{-3}	1.65×10^{-3}	1.65×10^{-3}
0.7	1.22×10^{-3}	1.22×10^{-3}	1.23×10^{-3}	5.69×10^{-4}	9.32×10^{-5}	4.65×10^{-4}	1.22×10^{-3}	1.22×10^{-3}	1.22×10^{-3}
0.8	8.07×10^{-4}	8.06×10^{-4}	8.13×10^{-4}	9.60×10^{-4}	4.65×10^{-4}	1.15×10^{-3}	8.05×10^{-4}	8.07×10^{-4}	8.05×10^{-4}
0.9	3.80×10^{-4}	3.79×10^{-4}	3.87×10^{-4}	1.40×10^{-3}	9.46×10^{-4}	2.18×10^{-3}	3.79×10^{-4}	3.80×10^{-4}	3.80×10^{-4}
1.0	5.40×10^{-8}	1.67×10^{-7}	7.86×10^{-6}	1.79×10^{-3}	1.25×10^{-3}	3.50×10^{-3}	2.27×10^{-9}	4.67×10^{-8}	3.32×10^{-8}

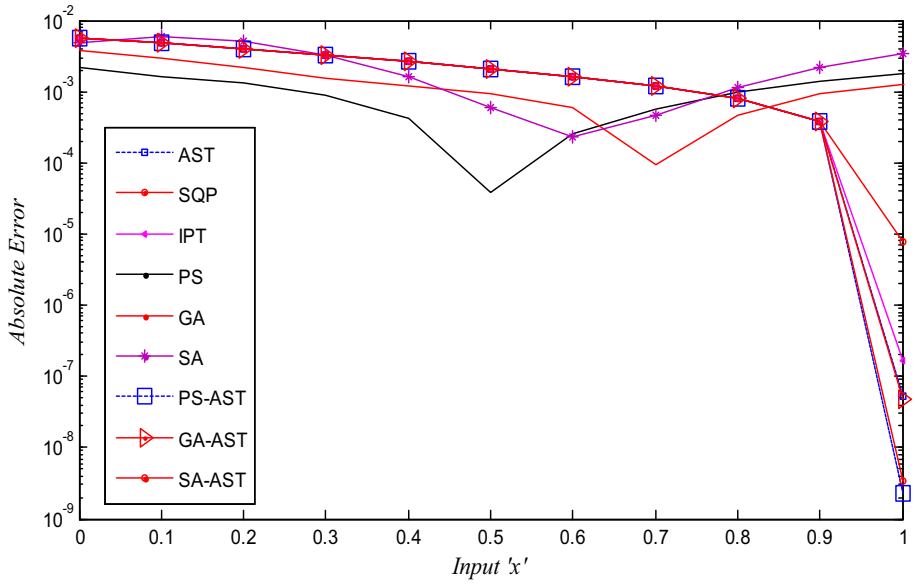

Fig. 7 Absolute errors for the proposed computing algorithms

The efficiency of the proposed solutions is further justified by using Monte Carlo simulations and their statistical analysis. The statistics by means of standard deviation (STD) and mean parameters are calculated in order to check the behaviour of the proposed solvers. Another metric based on the mean-square error is defined for 100 observations as

$$\mathrm{MSE} = \frac{1}{100}\sum_{i=0}^{100}\left(|u(x) - \hat{u}_i(x)|\right)^2 \tag{14}$$

where'i' is the index of independent runs of the solvers.

The descriptive statistical analyses for 100 runs of each scheme to solve the corneal shape model are conducted, and the results are tabulated in Table 5. It is seen that the results of the proposed scheme achieved reasonably accurate values based on minimum, maximum, mean, MAE, MSE and RMSE indicators.

The reliable and effective statistical method based on analysis of variance (ANOVA) is exploited to analyse the small variation in the results of proposed methodologies. Therefore, the average efficiency based on MAE values for each optimization technique has been analysed via descriptive statistical operators in terms of plots of the confidence intervals as well as ANOVA outcomes. Results of ANOVA analyses are graphically presented in Figs. 10 and 11 for 95% confidence interval and numerically tabulated in Table 6. It is seen that in case of 95% confidence interval plot of ANOVA, the performance of the hybrid scheme is slightly better than that of PS and GA performance on both accuracy operators of MAEs and AEs. The

Table 5 Statistical indicators of the different approaches for the corneal shape model

Method	x	Descriptive statistical analysis					
		Minimum	Maximum	Mean	MAE	MSE	RMSE
AST	0.0	0.005657	0.513958	0.010768	0.010768	0.002674	0.051706
	0.2	0.003973	0.488573	0.008837	0.008837	0.002403	0.094008
	0.4	0.002649	0.498503	0.007619	0.007619	0.002492	0.087286
	0.6	0.00164	0.540016	0.007035	0.007035	0.002919	0.083875
	0.8	0.000803	0.614654	0.006944	0.006944	0.003779	0.083332
SQP	0.0	0.005349	0.005764	0.00568	0.00568	3.23E−05	0.00568
	0.2	0.003706	0.004045	0.003986	0.003986	1.59E−05	0.003987
	0.4	0.002542	0.002679	0.002658	0.002658	7.06E−06	0.002658
	0.6	0.001523	0.001681	0.00165	0.00165	2.72E−06	0.00165
	0.8	0.000579	0.000831	0.000802	0.000802	6.44E−07	0.000803
IPT	0.0	0.005677	0.005698	0.005685	0.005685	3.23E−05	0.005685
	0.2	0.003986	0.004001	0.003991	0.003991	1.59E−05	0.003991
	0.4	0.002656	0.002664	0.00266	0.00266	7.08E−06	0.00266
	0.6	0.001648	0.001655	0.001651	0.001651	2.73E−06	0.001651
	0.8	0.000805	0.000807	0.000806	0.000806	6.49E−07	0.000806
PS	0.0	0.00062	0.006556	0.00501	0.00501	0.00501	0.005144
	0.2	0.000085	0.004634	0.003426	0.003426	0.003426	0.00355
	0.4	0.000415	0.004234	0.002273	0.002273	0.002273	0.002366
	0.6	4.52E−05	0.006812	0.001452	0.001452	0.001452	0.001724
	0.8	1.76E−06	9.71E−03	8.74E−04	0.000874	0.000874	0.001725
GA	0.0	0.001406	0.245335	0.008216	0.008216	0.000646	0.025421
	0.2	0.00213	0.238281	0.006723	0.006723	0.000603	0.024552
	0.4	0.000788	0.245346	0.005834	0.005834	0.000641	0.025322
	0.6	2.92E−05	0.263804	0.005473	0.005473	0.000752	0.027421
	0.8	7.49E−06	2.96E−01	5.50E−03	0.005497	0.000954	0.030883
SA	0.0	0.003872	0.305123	0.105186	0.105186	0.105186	0.129161
	0.2	0.001783	0.269699	0.087174	0.087174	0.087174	0.110189
	0.4	0.000379	0.266888	0.084959	0.084959	0.084959	0.107013
	0.6	0.000227	0.386658	0.097487	0.097487	0.097487	0.119672
	0.8	0.001154	0.653429	0.115119	0.115119	0.115119	0.145025
PS–AST	0.0	0.004143	0.0065	0.005678	0.005678	0.005678	0.005686
	0.2	0.002867	0.004583	0.003986	0.003986	0.003986	0.003992
	0.4	0.001919	0.003051	0.002657	0.002657	0.002657	0.002661
	0.6	0.001212	0.001883	0.001649	0.001649	0.001649	0.001652
	0.8	0.000606	0.000911	0.000805	0.000805	0.000805	0.000806
GA–AST	0.0	0.005621	0.005727	0.005683	0.005683	0.005683	0.005683
	0.2	0.003944	0.004019	0.00399	0.00399	0.00399	0.00399
	0.4	0.00263	0.002682	0.002659	0.002659	0.002659	0.002659
	0.6	0.001632	0.001665	0.001651	0.001651	0.001651	0.001651
	0.8	0.000797	0.000812	0.000806	0.000806	0.000806	0.000806
SA–AST	0.0	0.005483	0.00574	0.005685	0.005685	0.005685	0.005685
	0.2	0.003844	0.004027	0.003991	0.003991	0.003991	0.003991
	0.4	0.002549	0.002682	0.00266	0.00266	0.00266	0.00266
	0.6	0.001601	0.001675	0.001651	0.001651	0.001651	0.001651
	0.8	0.000747	0.000812	0.000804	0.000804	0.000804	0.000804

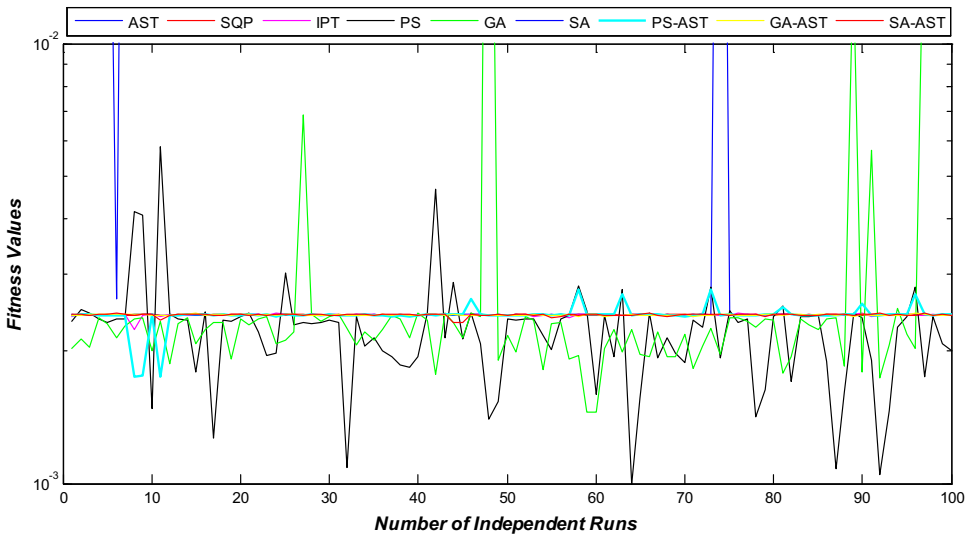

Fig. 8 Results of statistics on fitness for multiple runs of the proposed computing algorithms

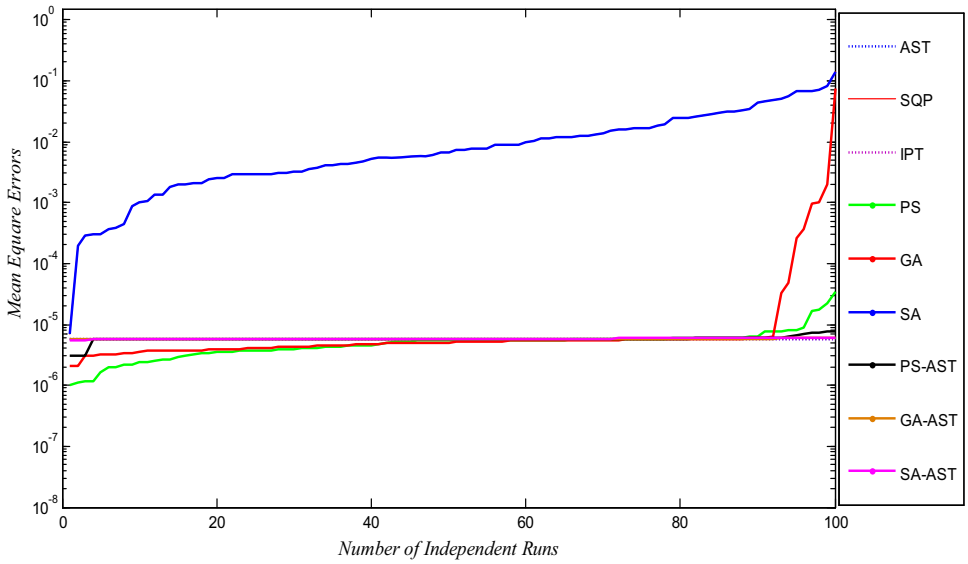

Fig. 9 Results of MSE for 100 runs

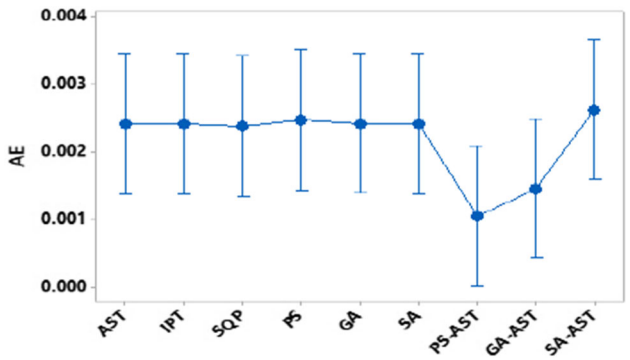

Fig. 10 Confidence intervals of 95% for ANOVA

comparative study on the basis of histogram illustrations is presented in Fig. 12, while two types of probability plots are shown in Figs. 13 and 14. Results presented in all these graphs show that each algorithm is effective with reasonable accuracy, but the performance of integrating computing solvers is relatively superior to the rest.

The computational complexity of six standalone algorithms AST, SQP, IPT, PS, GA and SA, as well as hybrid heuristic of PS–AST, GA–AST and SA–AST is analysed to determine the efficiency on the basis of multiple autonomous runs (100 runs). The computational averaged data in terms of execution times, iterations/generations executed and fitness functions evaluated are calculated for the analysis. The results are provided in Table 7 for all nine algorithms. These results show that AST algorithm is the most efficient in standalone methodologies with computation time around 6.45 ± 3 s, iterations around 340.5 ± 175 and fitness functions executed around $20{,}844 \pm 10{,}783$, while in combined computational heuristic GA–AST outperformed the rest with complexity

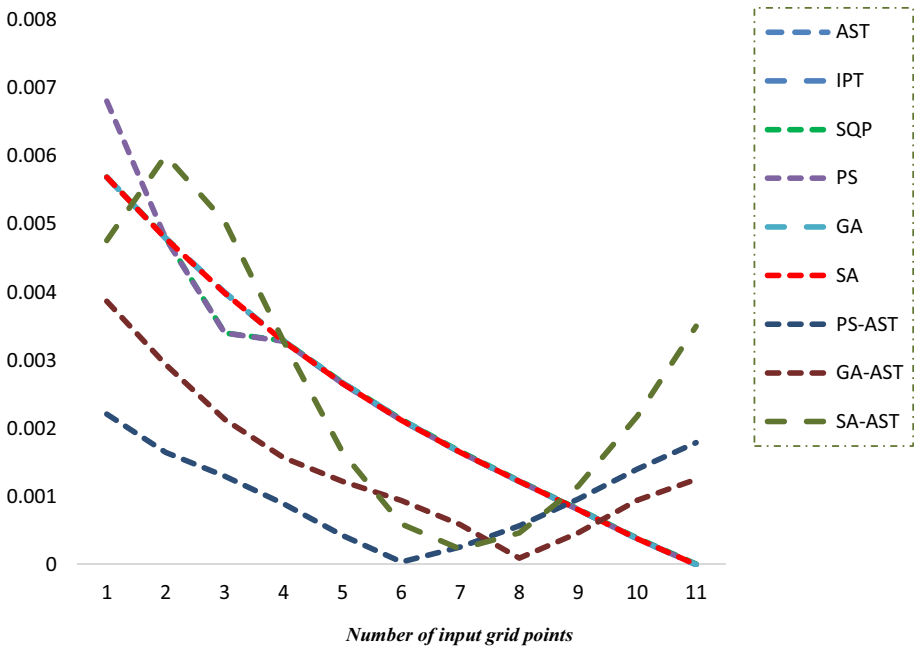

Fig. 11 Comparison on AE values calculated for 100 runs

indices around 189 ± 50, 2029 ± 635 and $508{,}267 \pm 133{,}710$. The results of all simulations are conducted on Dell Latitude E0420, Intel(R) Core(TM) i5-2520 M CPU 2.50 GHz, 6 GB RAM, running MATLAB 2018a on operating system Microsoft Window 10.

Table 6 Outcomes of the ANOVA test for each solver

Methodology
Null hypothesis: All means are set to be equal, **Alternative hypothesis:** At least one mean is statistically different **Significance level:** α = 0.05 with similar variances ere considered for the analyses.

Analysis of Variance

Source	DF	Adj SS	Adj MS	F-Value	P-Value
Factor	8	0.000026	0.000003	1.08	0.385
Error	90	0.000270	0.000003		
Total	98	0.000296			

Model Summary

S	R-sq	R-sq(adj)	R-sq(pred)
0.0017317	8.76%	0.65%	0.00%

Means

Factor	N	Mean	StDev	95% CI
AST	11	0.002418	0.001854	(0.001381, 0.003455)
IPT	11	0.002417	0.001853	(0.001380, 0.003454)
SQP	11	0.002371	0.001809	(0.001333, 0.003408)
PS	11	0.002465	0.002034	(0.001428, 0.003502)
GA	11	0.002422	0.001855	(0.001384, 0.003459)
SA	11	0.002417	0.001853	(0.001380, 0.003454)
PS-AST	11	0.001045	0.000689	(0.000007, 0.002082)
GA-AST	11	0.001456	0.001128	(0.000418, 0.002493)
SA-AST	11	0.002623	0.002022	(0.001586, 0.003661)

Pooled StDev = 0.00173165

Tukey Simultaneous 95% CIs

4 Conclusions

Integrated neuro-heuristic computing paradigm is presented to calculate the approximate results of BVPs arising in the modelling of the corneal shape using neural networks and their optimization with standalone methods AST, GA, SQP, IPT, PS and SA, along with the approximate solutions of hybrid schemes GA–AST, PS–AST and SA–AST. The comparison of the approximated results with the numerical solution obtained through an implicit Runge–Kutta method illustrates the validity of the proposed stochastic numerical solvers; however, hybrid methodologies achieved relatively better precision. The convergence analyses based on 100 autonomous runs for each solver also certify the performance of the stochastic solvers for reliable, viable and robust solutions of the mathematical model of the corneal shape. The ANOVA-based statistics show a better precision and performance of the PS- and GA-based standalone proposed stochastic methods on the basis of 95% confidence interval as well as error bar plots. Similarly, the hybrid scheme based on PS–AST and GA–AST provides better accuracy and convergence.

In future, one may exploit the strength of the proposed stochastic solvers as good alternatives for solving governing differential equations representing stiff and non-stiff applications of linear and nonlinear physical systems, particularly the complex mathematical models arising in bioinformatics [69–71].

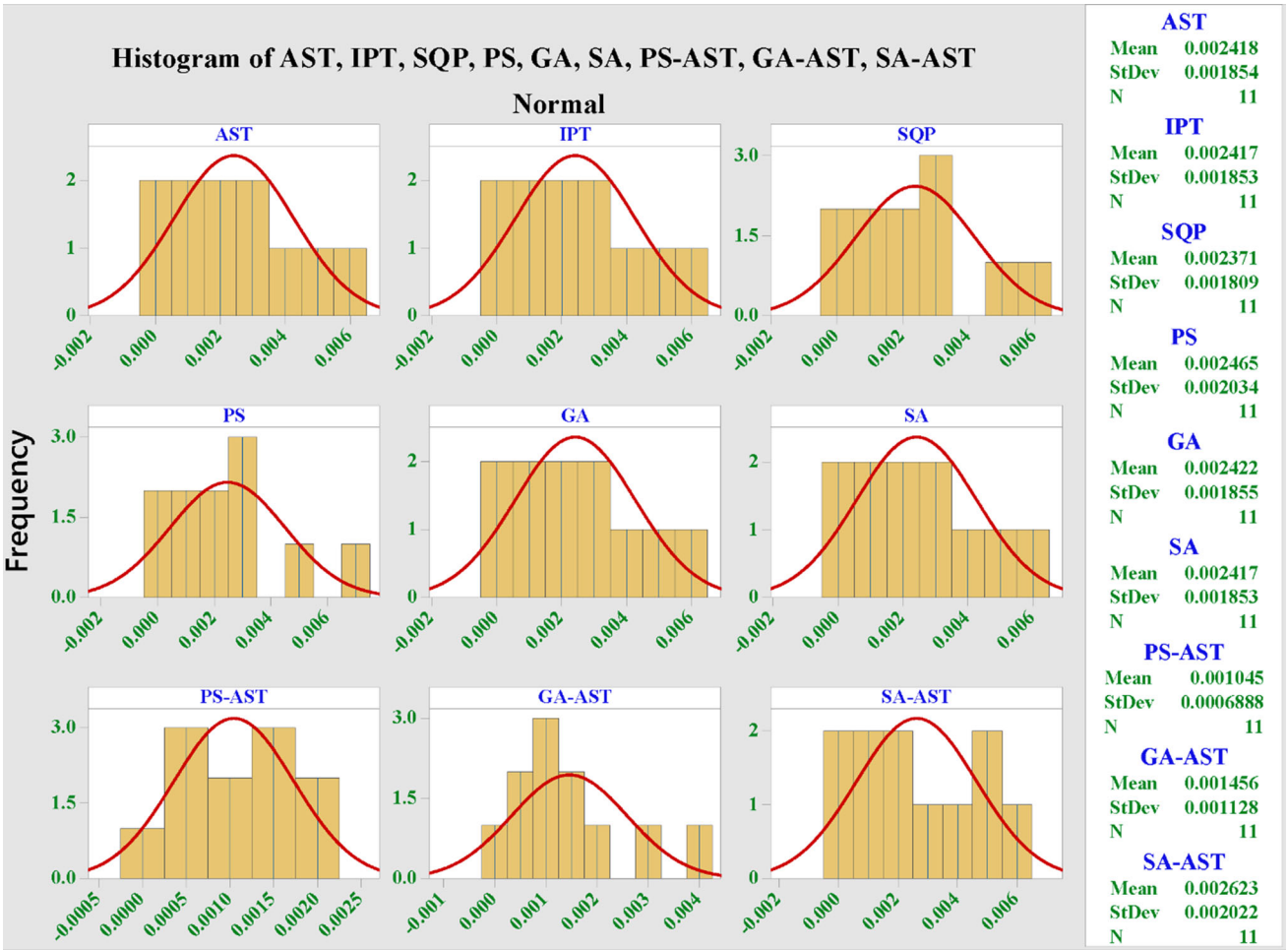

Fig. 12 Histograms illustrating the proposed approaches

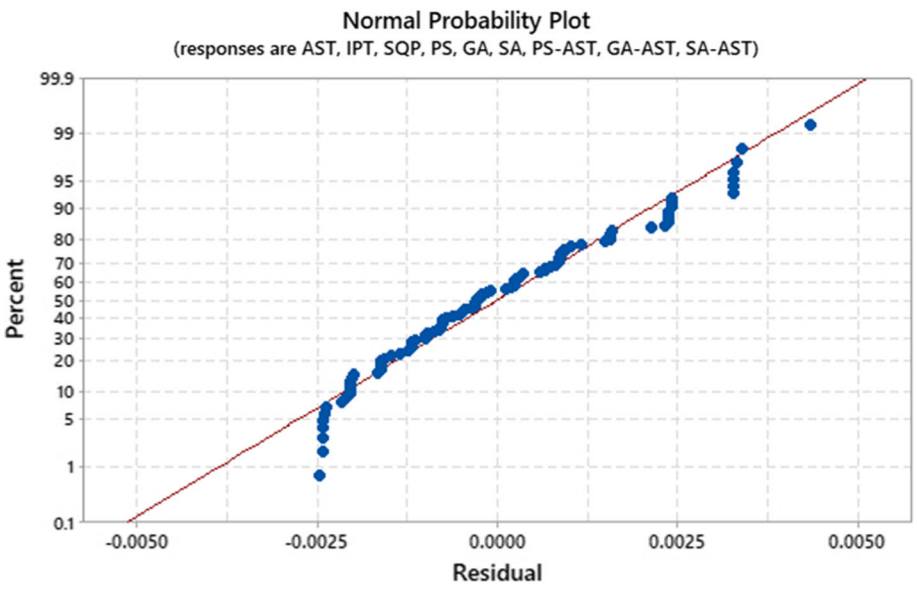

Fig. 13 Comparison through probabilities

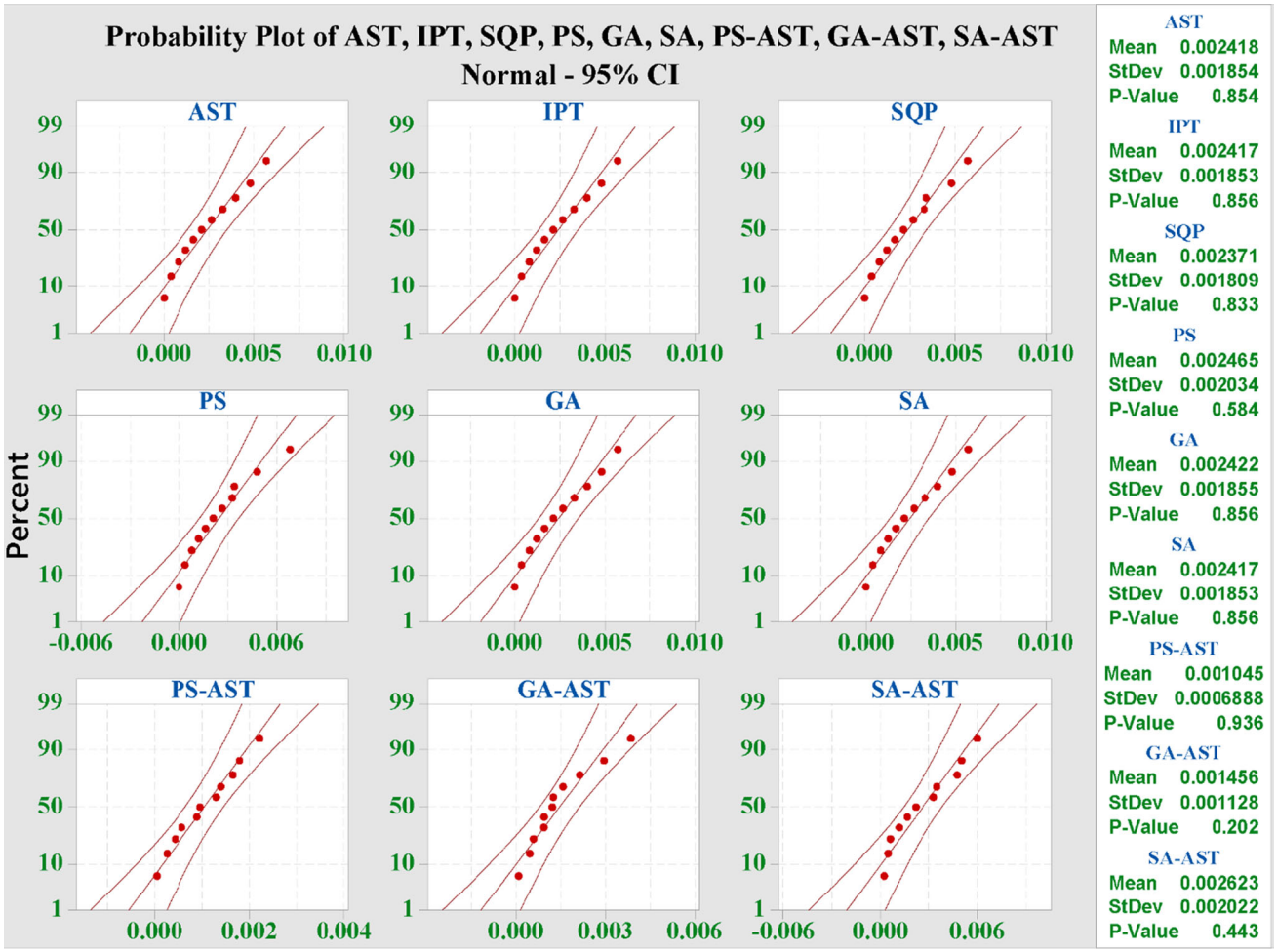

Fig. 14 Comparison through normal distribution of data for the proposed approaches

Table 7 Data on computational complexity

Index	Execution times		Iterations/generations		Functions executed	
	Values	Standard deviation	Values	Standard deviation	Values	Standard deviation
AST	6.45	3.19	340.50	175.99	20,844.10	107,83.55
IPT	18.41	1.91	800.00	0.00	50,284.10	958.14
SQP	19.27	7.38	800.00	0.00	63,978.00	21,660.22
PS	2371.89	692.40	214,381.10	42,180.55	9,424,659.80	1,819,385.46
GA	177.09	43.47	1606.90	397.03	482,370.00	119,108.73
SA	8552.57	597.87	1,000,001.00	0.00	1,152,948.00	545.67
PS–AST	2380.87	697.87	214,759.20	42,400.90	9,447,819.70	1,832,907.31
GA–AST	189.03	51.09	2029.60	635.22	508,267.60	133,710.41
SA–AST	8559.74	600.78	1,000,492.30	230.30	1,183,042.00	14,659.42

Acknowledgements The authors want to thank the anonymous referees for their careful reading of the manuscript and their comments, which greatly improved the final result.

Authors' contributions All authors contributed equally to this manuscript.

Funding Not applicable.

Compliance with ethical standards

Conflict of interest The authors declare that they have no conflict of interest.

References

1. Barbosa YM, Hernández DM (2001) A review of methods for measuring corneal topography. Optom Vis Sci 78:240–253
2. Okrasiński W, Płociniczak Ł (2013) Bessel function model of corneal topography. Appl Math Comput 223:36–443
3. Coelho I, Corsato C, Omari P (2014) A one-dimensional prescribed curvature equation modeling the corneal shape. Bound Value Probl 1:1–19
4. Okrasinski W, Płociniczak Ł (2012) A nonlinear mathematical model of the corneal shape. Nonlinear Anal Real World Appl 13:1498–1505
5. Mahavier WT, Hunt J (2006) An alternative mathematical algorithm for the photo and video keratoscope. Nonlinear Anal Real World Appl 7:1223–1232
6. Rosales MA, Aubry MJ, Olazagasti EL, Ibarra J, Tepichn E (2009) Anterior corneal profile with variable asphericity. Appl Opt 48:6594–6599
7. Anderson K, El-Sheikh A, Newson T (2004) Application of structural analysis to the mechanical behaviour of the cornea. J R Soc 1:3–15
8. Ahmed E (2010) Finite element modeling of corneal biomechanical behaviour. J Refract Surg 26:289–300
9. Iskander DR, Collins MJ, Davis B (2001) Optimal modeling of corneal surfaces by Zernike polynomials. IEEE Trans Biomed Eng 48:87–95
10. Schneider M, Iskander DR, Collins MJ (2009) Modeling corneal surfaces with rational functions for high-speed video keratoscopy data compression. IEEE Trans Biomed Eng 56:493–499
11. Urs R, Ho A, Manns F, Parel JM (2010) Age dependent Fourier model of the shape of the isolated ex vivo human crystalline lens. Vis Res 50:1041–1047
12. Bakaraju RC, Ehrmann K, Falk D, Ho A, Papas E (2010) Physical human model eye and methods of its use to analyse optical performance of soft contact lenses. Opt Express 18:16868–16882
13. Grytz R, Meschke G (2009) Constitutive modeling of crimped collagen fibrils in soft tissues. J Mech Behav Biomed Mater 2:522–533
14. Nee J (2010) Nonlinear integral equation from the BCS gap equations of superconductivity. Nonlinear Anal Real World Appl 11:190–197
15. Trattler W, Majmudar P, Luchs JI, Swartz T (2010) Cornea handbook. Slack Incorporated, Thorofare
16. Płociniczak L, Okrasiński W, Nieto JJ, Domínguez O (2014) On a nonlinear boundary value problem modeling corneal shape. J Math Anal Appl 414:461–471
17. Płociniczak L, Okrasiński W (2015) Nonlinear parameter identification in a corneal geometry model. Inverse Probl Sci Eng 23:443–456
18. Effati S, Pakdaman M (2010) Artificial neural network approach for solving fuzzy differential equations. Inf Sci 180(8):1434–1457
19. Baymani M, Effati S, Niazmand H, Kerayechian A (2015) Artificial neural network method for solving the Navier–Stokes equations. Neural Comput Appl 26(4):765–773
20. Aquino G, Rubio JDJ, Pacheco J, Gutierrez GJ, Ochoa G, Balcazar R, Cruz DR, Garcia E, Novoa JF, Zacarias A (2020) Novel nonlinear hypothesis for the delta parallel robot modeling. IEEE Access 8:46324–46334
21. Fateh MF et al (2017) Biologically inspired computing framework for solving two-point boundary value problems using differential evolution. Neural Comput Appl 28(8):2165–2179
22. de Jesús Rubio J (2009) SOFMLS: online self-organizing fuzzy modified least-squares network. IEEE Trans Fuzzy Syst 17(6):1296–1309
23. Majeed K et al (2017) A genetic algorithm optimized Morlet wavelet artificial neural network to study the dynamics of nonlinear Troesch's system. Appl Soft Comput 56:420–435
24. Elias I, Rubio JDJ, Cruz DR, Ochoa G, Novoa JF, Martinez DI, Muñiz S, Balcazar R, Garcia E, Juarez CF (2020) Hessian with mini-batches for electrical demand prediction. Appl Sci 10(6):2036
25. Meda-Campaña JA (2018) On the estimation and control of nonlinear systems with parametric uncertainties and noisy outputs. IEEE Access 6:31968–31973
26. Raja MAZ, Farooq U, Chaudhary NI, Wazwaz AM (2016) Stochastic numerical solver for nanofluidic problems containing multi-walled carbon nanotubes. Appl Soft Comput 38:561–586
27. Umar M et al (2019) Intelligent computing for numerical treatment of nonlinear prey–predator models. Appl Soft Comput 80:506–524
28. Raja MAZ, Ahmad I, Khan I, Syam MI, Wazwaz AM (2017) Neuro-heuristic computational intelligence for solving nonlinear pantograph systems. Front Inf Technol Electron Eng 18(4):464–484
29. Ahmad I et al (2019) Design of computational intelligent procedure for thermal analysis of porous fin model. Chin J Phys 59:641–655
30. Mehmood A et al (2019) Integrated intelligent computing paradigm for the dynamics of micropolar fluid flow with heat transfer in a permeable walled channel. Appl Soft Comput 79:139–162
31. Raja MAZ, Samar R, Alaidarous ES, Shivanian E (2016) Bio-inspired computing platform for reliable solution of Bratu-type equations arising in the modeling of electrically conducting solids. Appl Math Model 40(11–12):5964–5977
32. Khan JA et al (2015) Nature-inspired computing approach for solving non-linear singular Emden–Fowler problem arising in electromagnetic theory. Connect Sci 27(4):377–396
33. Raja MAZ (2014) Solution of the one-dimensional Bratu equation arising in the fuel ignition model using ANN optimised with PSO and SQP. Connect Sci 26(3):195–214
34. Yadav N, Yadav A, Kumar M, Kim JH (2017) An efficient algorithm based on artificial neural networks and particle swarm optimization for solution of nonlinear Troesch's problem. Neural Comput Appl 28(1):171–178
35. Raja MAZ (2014) Stochastic numerical treatment for solving Troesch's problem. Inf Sci 279:860–873
36. Ahmad I et al (2016) Bio-inspired computational heuristics to study Lane–Emden systems arising in astrophysics model. SpringerPlus 5(1):1866
37. Mehmood A, Zameer A, Aslam MS, Raja MAZ (2019) Design of nature-inspired heuristic paradigm for systems in nonlinear electrical circuits. Neural Comput Appl. https://doi.org/10.1007/s00521-019-04197-7
38. Sabir Z et al (2018) Neuro-heuristics for nonlinear singular Thomas–Fermi systems. Appl Soft Comput 65:152–169
39. Ahmad I et al (2017) Neural network methods to solve the Lane–Emden type equations arising in thermodynamic studies of the spherical gas cloud model. Neural Comput Appl 28(1):929–944
40. Ahmad I et al (2018) Neuro-evolutionary computing paradigm for Painlevé equation-II in nonlinear optics. Eur Phys J Plus 133(5):184
41. Raja MAZ, Shah FH, Syam MI (2018) Intelligent computing approach to solve the nonlinear Van der Pol system for heartbeat model. Neural Comput Appl 30(12):3651–3675

42. Raja MAZ, Asma K, Aslam MS (2017) Bio-inspired computational heuristics to study models of HIV infection of CD4 + T-cell. Int J Biomath 11(2):1850019. https://doi.org/10.1142/S1793524518500195
43. Munir A et al (2019) Intelligent computing approach to analyze the dynamics of wire coating with Oldroyd 8-constant fluid. Neural Comput Appl 31(3):751–775
44. Raja MAZ, Shah Z, Manzar MA, Ahmad I, Baleanu D (2018) A new stochastic computing paradigm for nonlinear Painlevé II systems in applications of random matrix theory. Eur Phys J Plus 133(7):254
45. Yadav N, Yadav A, Deep K (2015) Artificial neural network technique for solution of nonlinear elliptic boundary value problems. In: Proceedings of fourth international conference on soft computing for problem solving, Springer India pp 113–121
46. Raja MAZ, Samar R, Manzar MA, Shah SM (2017) Design of unsupervised fractional neural network model optimized with interior point algorithm for solving Bagley–Torvik equation. Math Comput Simul 132:139–158
47. Raja MAZ, Azad S, Shah SM (2017) Bio-inspired computational heuristics to study the boundary layer flow of the Falkner–Scan system with mass transfer and wall stretching. Appl Soft Comput 57:293–314
48. Raja MAZ, Khan JA, Chaudhary NI, Shivanian E (2016) Reliable numerical treatment of nonlinear singular Flierl–Petviashivili equations for unbounded domain using ANN, GAs, and SQP. Appl Soft Comput 38:617–636
49. Raja MAZ, Manzar MA, Samar R (2015) An efficient computational intelligence approach for solving fractional order Riccati equations using ANN and SQP. Appl Math Model 39(10):3075–3093
50. Raja MAZ, Khan JA, Shah SM, Samar R, Behloul D (2015) Comparison of three unsupervised neural network models for first Painlevé Transcendent. Neural Comput Appl 26(5):1055–1071
51. Raja MAZ, Samar R, Rashidi MM (2014) Application of three unsupervised neural network models to singular nonlinear BVP of transformed 2D Bratu equation. Neural Comput Appl 25(7–8):1585–1601
52. Hager WW, Zhang H (2006) A new active set algorithm for box constrained optimization. SIAM J Optim 17:526–557
53. Achache M, Tabchouche N (2019) A full-Newton step feasible interior-point algorithm for monotone horizontal linear complementarity problems. Optim Lett 13(5):1039–1057
54. Darvay Z, Rigó PR (2018) New interior-point algorithm for symmetric optimization based on a positive-asymptotic barrier function. Numer Funct Anal Optim 39(15):1705–1726
55. Kirkpatrick S, Gelatt CD, Vecchi M (1983) Optimization by simulated annealing. Science 220(4598):498–516
56. Cenny V (1985) Thermodynamical approach to the traveling salesman problem an efficient simulation algorithm. J Optim Theory Appl 45(1):41–51
57. Vincent FY, Redi AP, Hidayat YA, Wibowo OJ (2017) A simulated annealing heuristic for the hybrid vehicle routing problem. Appl Soft Comput 53:119–132
58. Wei L, Zhang Z, Zhang D, Leung SC (2018) A simulated annealing algorithm for the capacitated vehicle routing problem with two-dimensional loading constraints. Eur J Oper Res 265(3):843–859
59. Kadhim AZM, Ali SK, Kassim MM (2018) Solving machine scheduling problem under fuzzy processing time using the simulated annealing method. J Progr Res Math 14(1):2308–2317
60. Hooke R, Jeeves TA (1961) Direct search solution of numerical and statistical problems. J Assoc Comput Mach (ACM) 8(2):212–229
61. Yu WC (1979) Positive basis and a class of direct search techniques. Sci Sin 9:53–67
62. Dolan ED, Lewis RM, Torczon VJ (2003) On the local convergence of pattern search. SIAM J Optim 14(2):567–583
63. Lewis RM, Torczon V (1999) Pattern search algorithms for bound con-strained minimization. SIAM J Optim 9(4):1082–1099
64. Holland JH (1992) Genetic algorithms. Sci Am 267(1):66–73
65. Araújo RDB, Coelho AA (2018) Hybridization of IMC and PID control structures based on filtered GPC using genetic algorithm. Comput Appl Math 37(2):2152–2165
66. Shahdi-Pashaki S, Teymourian E, Tavakkoli-Moghaddam R (2018) New approach based on group technology for the consolidation problem in cloud computing-mathematical model and genetic algorithm. Comput Appl Math 37(1):693–718
67. de Fatima Brondani M, Sausen ATZR, Sausen PS, Binelo MO (2018) Parameter estimation of lithium ion polymer battery mathematical model using genetic algorithm. Comput Appl Math 37:296–313
68. Yuxin Z, Shenghong L, Feng J (2017) Overlapping community detection in complex networks using multi-objective evolutionary algorithm. Comput Appl Math 36(1):749–768
69. Raja MAZ, Shah FH, Alaidarous ES, Syam MI (2017) Design of bio-inspired heuristic technique integrated with interior-point algorithm to analyze the dynamics of heartbeat model. Appl Soft Comput 52:605–629. https://doi.org/10.1016/j.asoc.2016.10.009
70. Raja MAZ, Umar M, Sabir Z, Khan JA, Baleanu D (2018) A new stochastic computing paradigm for the dynamics of nonlinear singular heat conduction model of the human head. Eur Phys J Plus 133(9):364. https://doi.org/10.1140/epjp/i2018-12153-4
71. Ahmad I et al (2019) Novel applications of intelligent computing paradigms for the analysis of nonlinear reactive transport model of the fluid in soft tissues and microvessels. Neural Comput Appl 31(12):9041–9059